Earth, Planets and Space

FULL PAPER

Open Access

Simultaneous equatorial plasma bubble observation using amplitude scintillations from GNSS and LEO satellites in low-latitude region

Khanitin Seechai[1], Lin Min Min Myint[1*], Kornyanat Hozumi[2], Michi Nishioka[2], Susumu Saito[3], Mamoru Yamamoto[4] and Pornchai Supnithi[1]

Abstract

This study estimates the scale sizes of the plasma density irregularities and the longitudinal width associated with equatorial plasma bubbles (EPBs) in equatorial and low-latitude regions. By analyzing amplitude scintillation S_4 indices and total electron content (TEC) measured from low earth orbit (LEO) satellite's beacon signals with 400 MHz and Global Navigation Satellite System (GNSS) L1/E1 signals with 1575.42 MHz, recorded by receivers at the KMITL station in Bangkok, Thailand (geographic; 13.73° N, 100.77°E, magnetic: 7.26°N), we investigate the characteristics of these irregularities. We collected data of 154 LEO satellite pass events during nighttime on 21 disturbed days in four equinoctial months in 2021. Based on the presence or absence of the scintillation effects on GNSS and LEO beacon signals, the events are categorized into four classes to estimate the scale size of the plasma density irregularities. The analysis suggests that events with both GNSS and LEO scintillations, as well as events with GNSS scintillation alone, occur predominantly before midnight assuming the presence of the small-scale size of the irregularities within EPB. However, events with only LEO scintillation occur throughout the whole night and some events are observed before the events with both GNSS and LEO scintillations. Post-sunset LEO scintillation alone may be attributed to the onset of EPBs developing at low altitude, while post-midnight LEO scintillation events near the magnetic equator, observed during periods of low GNSS Rate of TEC Index (ROTI) values, are associated with bottom-side ionospheric irregularities but are not linked with EPB. The findings are consistent with previous researches on the generation and decay of electron density irregularities within plasma bubbles. However, this study provides new insights by using specific data sets and analysis techniques, offering a more comprehensive understanding of the association of LEO scintillations with bottom-side ionospheric irregularities near the magnetic equator, not observed in the ROTI map.

Keywords Space weather, Global Navigation Satellite System, Low earth orbit satellites, TEC, Ionospheric irregularity, Equatorial plasma bubble, Amplitude scintillation index

*Correspondence:
Lin Min Min Myint
linminmin.my@kmitl.ac.th
Full list of author information is available at the end of the article

Graphical Abstract

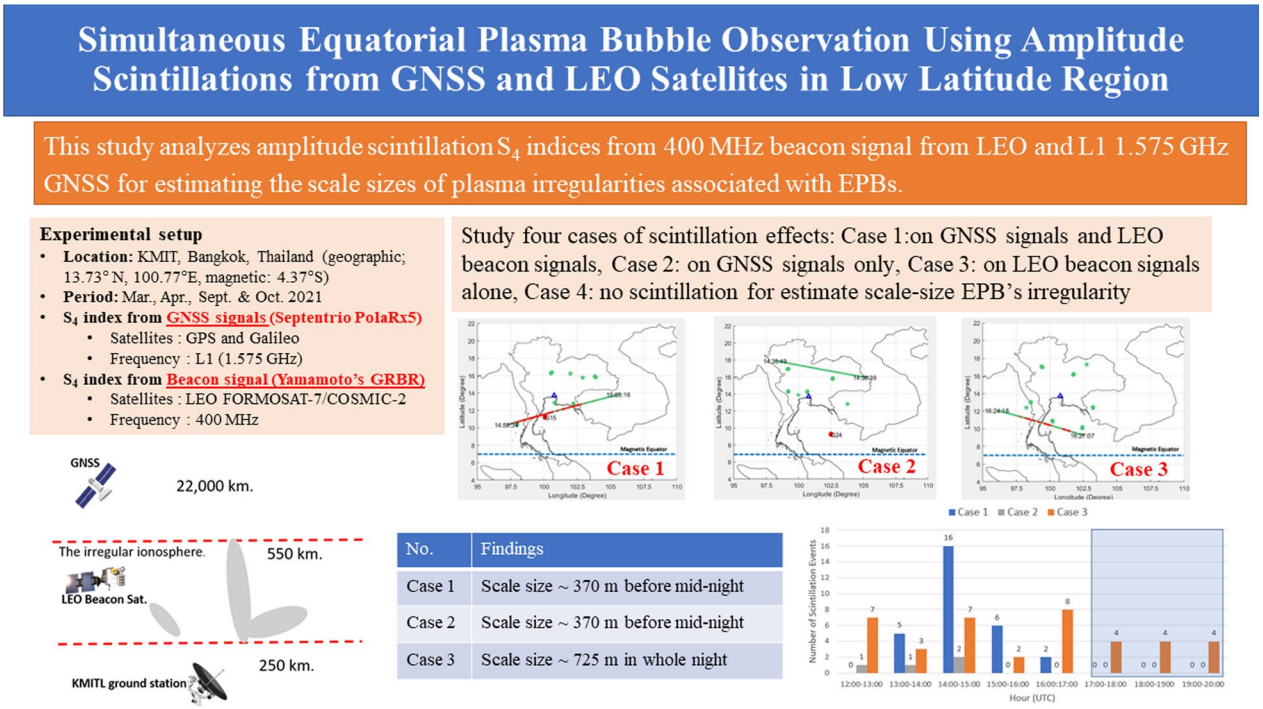

Introduction

Ionospheric scintillation refers to rapid fluctuations in the amplitude and phase of radio signals that pass through the ionospheric plasma density irregularities (Kung Chie Yeh and Chao-Han Liu 1982). Specifically, amplitude scintillations are frequently detected in the satellite signal near the magnetic equator and at low latitudes, where equatorial plasma bubbles (EPBs) are often observed (de Oliveira Moraes et al. 2012). EPBs have zonal widths ranging from tens to hundreds of kilometers in the magnetic east–west direction and plasma density irregularities associated with the EPB can have scale sizes ranging from tens of meters to a few kilometers (Yokoyama et al. 2014; Tsunoda 2015; Bhattacharyya 2022). Understanding the causes of scintillations related to EPBs is vital for space weather studies, and technologies related to satellite communication and navigation systems (Kintner 2009).

Within EPBs, plasma density irregularities with scale sizes close to the first Fresnel scale ($d_F = \sqrt{2\lambda h}$ where λ is the wavelength of the radio signal and h is the altitude of the ionospheric irregularity layer) induce amplitude scintillations in satellite signals (Bhattacharyya et al. 2000; Yang and Liu 2016). Particularly, small and intermediate-scale plasma irregularities (less than 1 km), can cause moderate-to-severe amplitude scintillations on radio signals within the very high frequency–ultra high frequency (VHF–UHF) band, including the Global Navigation Satellite System (GNSS) signals (Kintner 2009; Li et al. 2021; Salles et al. 2021).

The study of space weather study observes the spatial and temporal variations of ionospheric electron content (TEC) and scintillations using GNSS signals from medium-earth orbit (MEO) satellites and VHF beacon signals from low earth orbit (LEO) satellites. Yamamoto (2008) developed the "GNU Radio Beacon Receiver (GRBR)" system using LEO satellite beacon signals of 150 and 400 MHz to measure ionospheric TEC and scintillations. TEC data from multi-constellation GNSS satellite signals provide a better perceptional understanding of the ionospheric temporal variation, whereas scanning along an LEO satellite trace provides high spatial resolution for capturing ionospheric structures (Watthanasangmechai et al. 2016).

The intensity of scintillation in the satellite signals is proportional to the electron density irregularities having a scale size corresponding to the Fresnel scale. The S_4 index is commonly used to measure the amplitude scintillation intensity in ground-based received signal, defined as the standard deviation of the received signal

power normalized by its mean value (Xiong et al. 2007). Analyzing scintillations from various frequency signals measured by the ground receivers provides valuable insights into prediction the scale sizes of the ionospheric irregularities associated with EPBs in the low-latitude region, while TEC variations from LEO satellites reveal the detailed structure of the EPB. However, due to the longitudinal and temporal variability of EPB characteristics and scintillation occurrences, further study is required to investigate the scintillation effects caused by EPB at low-latitude region, over Thailand.

In this study, we use amplitude scintillation S_4 indices from both the LEO F7/C2 satellite's beacon signals at 400 MHz through a GRBR receiver (Yamamoto 2008), and GNSS satellite's L1 or E1 signals at 1575.42 MHz recorded by a GNSS receiver at KMITL Bangkok station, Thailand, which is in the low-latitude region. We focused only on the scintillation events occurring during magnetically quiet conditions with Kp < 3. By observing the presence or absence of the scintillation effects on signals with different frequencies, we estimate the scale size of the plasma irregularities associated with EPBs because the scale size of the irregularities generating the scintillations corresponds to the Fresnel scale, which is determined by the wavelength or frequency of the signal that passes through irregularities. We analyzed the occurrence of the observed scintillation events in the four cases: scintillations on both GNSS L1/E1 signal and LEO beacon signal, scintillations on GNSS L1/E1 signals alone, and scintillations on LEO beacon signal only, and no scintillation. Investigating one sample event from each of the enhanced scintillation cases, we examined the internal structure of the electron density-depleted region in each case by observing the relative TEC and its standard deviation from the GRBR beacon receiver. Finally, we summarized the occurrence frequency distribution and duration of all scintillation events.

Theoretical background and data

When a radio signal passes through ionospheric plasma density irregularities with scale sizes below the first Fresnel zone, it experiences phase modulation, resulting in interference patterns or scintillations on the ground (Ghobadi et al. 2020). In low-latitude regions, these ionospheric irregularities are associated with EPBs or bottom-side ionospheric instabilities (Tsunoda 2015; Bhattacharyya 2022). Scintillation, even at moderate intensity, can degrade the accuracy and integrity of GNSS positioning (Kintner 2009; Salles et al. 2021). Therefore, there have been studies on the scintillation effects on multi-frequency GNSS signals in low-latitude regions (Rama Rao et al. 2006; Oliveira Moraes et al. 2017; Bumrungkit et al. 2022).

The characteristics of EPBs have been extensively studied using various data from multiple instruments, including GNSS receivers (Otsuka 2018; Joshi et al. 2019; Li et al. 2021). Buhari et al. (2014) and Manga et al. (2021) studied the two-dimensional structure of EBPs using the rate of total electron content change index (ROTI) data from a dense GNSS receiver network, as ROTI serves a reliable indicator of scintillation events. Additionally, VHF beacon signals from LEO satellites are employed to observe TEC variations due to their ability to scan ionospheric structures with a high spatial resolution. Using GRBR system developed by Yamamoto (2008), the latitudinal ionosphere structure was observed in (Watthanasangmechai et al. 2014) and the relationship between the large-scale wave structure (LSWS) and EPB occurrence was examined in (Liow et al. 2019). Moreover, Seechai et al. (2022) found that amplitude scintillations occurred more frequently on the beacon signal recorded on GRBR receiver than on GNSS signal because irregularities with smaller scale size have shorter lifetimes than the larger ones (Otsuka et al. 2009; Li et al. 2021).

In this study, we employed two types of receivers to measure S_4 indices of LEO satellite signals and GNSS satellite signals. The location of the receivers is at the KMITL Bangkok station (geographic; 13.73°N, 100.77°E, magnetic: 7.26°N), Thailand. The first receiver used is an open-source digital beacon receiver called GRBR, developed by Yamamoto (2008). The GRBR receiver information is publicly available at the URL https://www.rish.kyoto-u.ac.jp/~yamamoto/digitalbeacon/. The receiver stores data during the satellite passes, which are then analyzed by an off-line data analysis program. The GRBR receiver computes the S_4 index with a 1-second resolution, and relative TEC values and their standard deviation values with a 0.1-second resolution. Recently, the GRBR receiver was modified to receive two beacon signals (400 MHz, 965 MHz) from the FORMOSAT-7/COSMIC-2 (F7/C2) constellation as explained in Hsiao et al. (2022). The GNSS receiver is a Septentrio PolaRx5 GNSS receiver, which computes S_4 index from the standard deviation of the 50-Hz raw signal power samples normalized to the average signal power over an 60-second interval. This study focused on the 400-MHz beacon signal from F7C2 LEO satellite and L1 frequency (1,575.42 MHz) signal from two GNSS constellations, GPS and Galileo satellites. The F7/C2 satellites orbit the Earth at approximately 550 km altitude with a 24-degree inclination for about 97 min (Taiwan Space Agency 2023), while GNSS satellites orbit at an altitude of 22,000 km for 12 h.

During the study period from post-sunset up to post-midnight hours, the GRBR receiver detected up to nine LEO satellite passes at different times, each lasting about

5 min or less. We examined the S_4 indices of the beacon and GNSS signals recorded by the receivers during each LEO satellite passing event over 21 days with EPB events in the equinox months (March, April, September and October of 2021) with elevation angles above 30 degrees to remove multipath effects. Our study focuses scintillation effects on magnetically quiet days with Kp ≤ 3 because scintillation events can still occur during magnetically quiet periods in the low-latitude region (Groves et al. 1997).

The S_4 index, which measures scintillation in satellite signals, is normally computed as:

$$S_4 = \sqrt{\frac{\langle I^2 \rangle - \langle I \rangle^2}{\langle I \rangle^2}}, \tag{1}$$

where I is the intensity of the trans-ionosphere signal and $\langle \cdot \rangle$ indicates the average over the interval of time of 1 min (Kung Chie Yeh and Chao-Han Liu 1982). However, the S_4 index in the GRBR receiver is estimated the ratio of the standard deviation and the average of the received power from the satellite's beacon signal at the receiver, i.e.:

$$S_{4,\mathrm{GRBR}} = \frac{\mathrm{std}(P_b)}{\mathrm{avg}(P_b)}, \tag{2}$$

and the received power of the beacon signal at the receiver, P_b is calculated as:

$$P_b = I_b^2 + Q_b^2, \tag{3}$$

where I_b and Q_b are the in-phase and quadrature-phase components of the received signal by the receiver.

In this study, we use a threshold of 0.8 for beacon signals based on the empirical study because the S_4 index from GRBR receiver during quiet time or daytime are mostly high as shown Fig. 1 where S_4 indices measured from two F7/C2 LEO satellites, F7 Flight Module 1 (F7 FM1) and F7 FM4 on 30 March 2021 (DOY 089), as recorded by the KMITL Bangkok station for approximately 3 min at different coordinated (UTC times), around 15:00 and 20:22, are illustrated. This study determined enhanced scintillation events when the S_4 value exceeds 0.8 continuously for a period of 5 s or longer. Figure 1a and b are the examples of enhanced scintillation event ($S_4 > 0.8$) and no significant scintillation event ($S_4 < 0.8$), respectively.

Similarly, for GNSS signals, we set a threshold of S_4 index to 0.2 like in Abadi et al. (2014) to identify an enhanced scintillation event as depicted in Fig. 2 which displays S_4 index values recorded by the KMITL Bangkok station during nighttime on 30 March 2021 (DOY 089) for different GNSS constellation satellites, with each color representing a different satellite. Between 13:30 and 15:00 UTC, the S_4 index values from multiple GNSS satellites are higher than the defined threshold, while weak or no scintillations were observed for the remaining time.

TEC values from GNSS signals are estimated using a geometry-free combination method that utilizes both

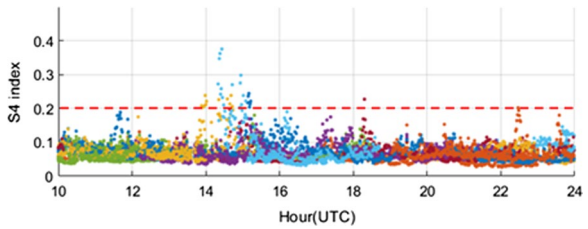

Fig. 2 S_4 index plot from GNSS satellite signals recorded by a receiver at the KMITL Bangkok station on 30 March 2021 (DOY 089) where different colors represent different satellites

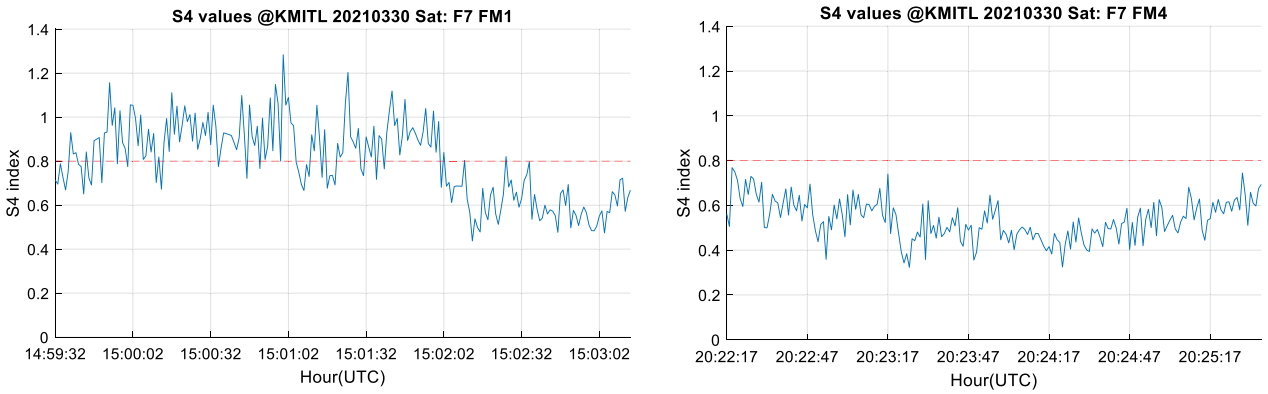

Fig. 1 S_4 index plots from **a** LEO F7 FM1 satellite during enhanced scintillation event and **b** F7 FM4 satellite during low scintillation event on 30 March 2021 (DOY 089) during quiet time

code and carrier-phase pseudoranges of dual-frequency signals from GNSS satellites (Krypiak-Gregorczyk and Wielgosz 2018). On the other hand, TEC values from beacon signals are computed using the relative TEC estimating method proposed by Watthanasangmechai et al. (2014). The standard deviation of the relative TEC in the GRBR receiver is computed using a window size of 10. For GNSS receiver, ROTI is the standard deviation of rate of TEC where the TEC is measured in unit of TECu (1 TECu = 10^{16} electrons/m^2) and ROTI is in unit of TECu/min. To compute the ROTI from GNSS signals for 5 min interval, we use Eq. (2) from (Pi et al. 1997):

$$\mathrm{ROTI} = \sqrt{\langle ROT^2 \rangle - \langle ROT \rangle^2}, \tag{4}$$

where ROT is the rate of TEC which is the difference in TEC between two consecutive intervals of 60 s. In this study, we used the GNSS ROTI map developed by a GNSS receiver network under the KMITL's Excellence Center in GNSS and Space Weather, (http://iono-gnss.kmitl.ac.th/) to check the locations and the area of the ionospheric irregularities over Thailand.

Results and discussion

In this work, we analyzed the scintillation S_4 indices of the LEO F7/C2 satellite's beacon signals at a frequency of 400 MHz and the GNSS satellite's L1/E1 signals with a frequency of 1575.42 MHz recorded by the receivers at KMITL Bangkok station, Thailand, in the low-latitude region. Theoretically, the amplitude scintillation is caused by irregularities with scale sizes close to the first Fresnel zone of the signal. With the peak of the ionospheric electron density irregularity was at 350 km altitude, the first Fresnel zones are approximately 370 m for L1, and 725 m for 400 MHz, respectively.

By observing the presence or absence of enhanced scintillations on these signals with different frequencies, we estimate the scale sizes of plasma irregularities in EPBs over Thailand. Measurements from the LEO satellite can observe the zonal width (east–west direction) of the EPBs along the satellite trajectory within a short time; therefore, we also analyzed the scintillation S_4 index and relative TEC values from the LEO signals to identify the longitudinal width of plasma-depleted regions inside EPBs.

The GRBR receiver detects multiple LEO satellite passes at different times. For each LEO satellite passing event, we examined the scintillation S_4 indices of both the beacon and GNSS signals recorded by the receivers during the nighttime. Based on the results, we classified into four cases as described in Table 1: Case 1) scintillations on both GNSS L1/E1 signal and LEO beacon signal; Case 2) scintillations on GNSS L1/E1 signals alone; Case 3) scintillations on LEO beacon signal only; and Case 4) no scintillation. We examined one sample event form each scintillation case and then summarized all cases of 154 events.

Table 1 Four cases of the scintillation events

Case	GNSS signal's S_4	Beacon signal's S_4
I	Greater than 0.2	Greater than 0.8
II	Greater than 0.2	Less than 0.8
III	Less than 0.2	Greater than 0.8
IV	Less than 0.2	Less than 0.8

Case 1: scintillations on both GNSS signal and beacon signals (DOY 089, 2021)

A Case 1 scintillation event was recorded from the LEO F7 FM4 satellite passing between 14:59:34 and 15:03:16 UTC (21:59:34–22:03:16 LT) on 30 March 2021 (DOY 089). Figure 3a shows scintillation levels at the IPPs (referenced to 350 km altitude) from the beacon signals (line), the GPS L1 signals (circle), and the Galileo E1 signals (star), recorded by the receivers at the KMITL Bangkok station. Enhanced scintillations were observed on both the L1 signal from a GPS satellite (G15) and the beacon signal from the LEO satellite, indicated by red color. We hypothesize that enhanced scintillation on the GNSS signal was caused by the small-scale irregularities (approximately 370 m) of EPBs. Figure 3b shows the ROIT map at 15:00 UTC (22:00 LT) over Thailand confirming that the LEO satellite passed through the area affected by EPBs, indicated by a red circle.

We also examined the values of S_4 index (top) against the relative TEC values and their standard deviation (bottom) derived from the beacon signal as shown in Fig. 4. Enhanced scintillations were detected between 14:59:38 UTC (@ E97.4999°) and 15:02:02 UTC (@ E102.8900°). The TEC profile plot revealed a plasma depletion region (between two red dashed lines) between two steep gradients of ionospheric Rel-TEC at 15:00:38 UTC (@ E99.7684°) and 15:01:42 UTC (@ E102.1400°). Based on this observation, we estimated that the EPB's longitudinal width about ~ 260 km (2.37° longitudinal range).

When comparing the TEC fluctuations during the enhanced scintillation period and low scintillation period, even small TEC fluctuations could still lead to the scintillation effect on the beacon signal with lower frequency. Thus, the enhanced S_4 index values in Figs. 3 and 4 enabled us to estimate the scale sizes of the plasma irregularities (approximately 370 m) associated EPB that can trigger GNSS scintillations, and the longitudinal

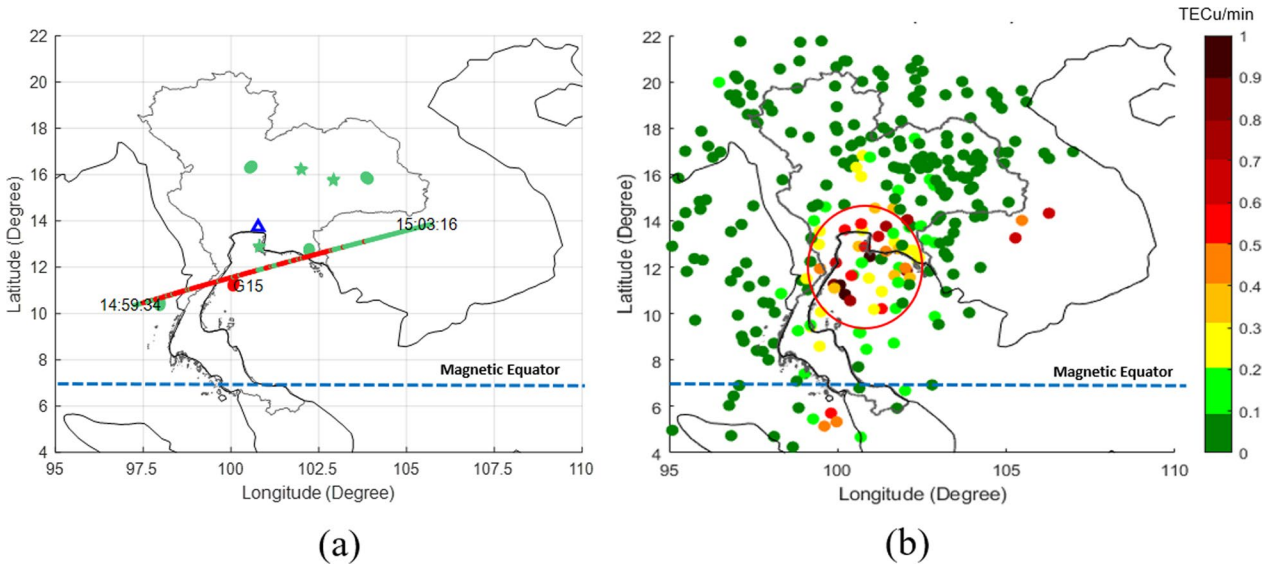

Fig. 3 Maps of ionospheric pierce points (IPPs) of **a** S_4 index of GNSS [GPS (circle) + Galileo(star)] and LEO satellite signals received at the KMITL Bangkok station and **b** ROTI map of GNSS signals from the KMITL's receiver network over Thailand around 15:00 UTC (22:00 LT) on 30 March 2021 (DOY 089) and red color refers to enhanced scintillation (higher than the threshold)

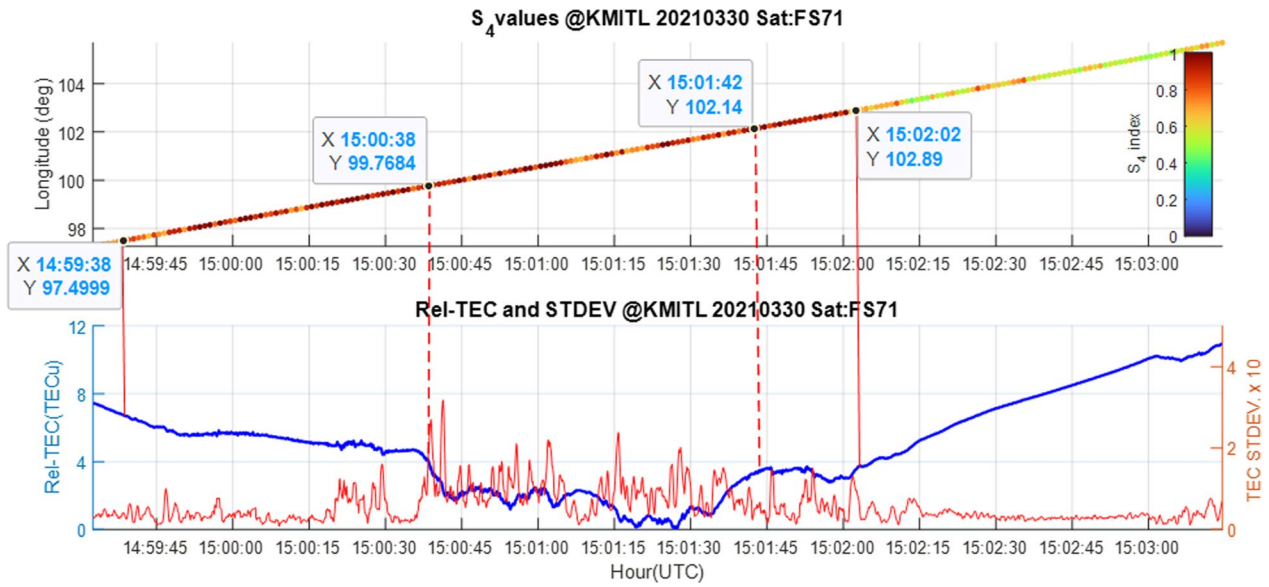

Fig. 4 S_4 index (top) values against the IPP along the LEO satellite's trajectory vs UTC time, the time profile plots of the relative TEC value and its standard deviation (bottom) during the satellite pass between 14:59 and 15:03 UTC (21:59–22:03 LT) on 30 March 2021 (DOY 089)

width of the plasma-depleted region of the EPB in the scintillation event of Case 1.

Case 2: scintillations on GNSS signal only (DOY 280, 2021)

During the pass of the LEO F7 FM2 satellite between 14:35:49 and 14:38:39 UTC (21:35:49–21:38:39 LT) on 28 April 2021 (DOY 118), enhanced scintillations in the E1 signal from a Galileo satellite (G2) or Case 2 events were recorded at the KMITL Bangkok station as shown in Fig. 5a. We assume that this GNSS scintillation was triggered by small-scale irregularities (approximately 370 m) associated with EPB near magnetic equator. Although the GNSS E1 signal is affected, no scintillation was observed on the signal of the LEO satellite, which orbited at higher latitudes. The ROTI map in Fig. 5b shows a small area of ionospheric disturbances in close proximity

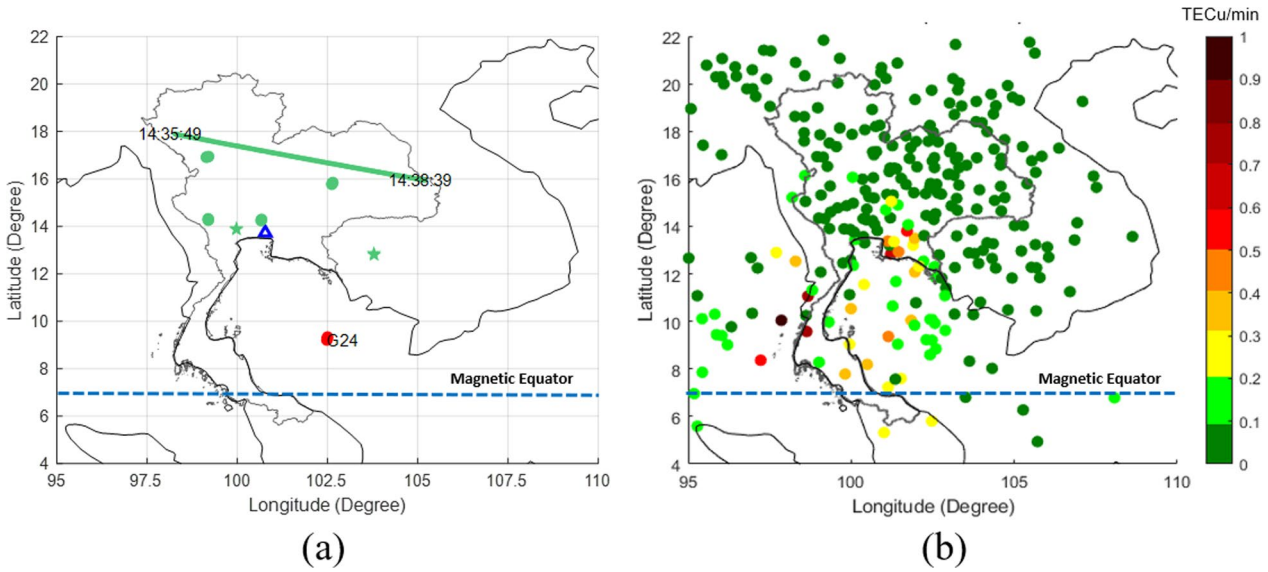

Fig. 5 Maps of ionospheric pierce points (IPPs) of **a** S_4 index of GNSS [GPS (circle)] and LEO satellite signals received at the KMITL Bangkok station and **b** ROTI map of GNSS signals from the KMITL's receiver network over Thailand around 14:35 UTC (21:35 LT) on 28 April 2021 (DOY 118) and red color refers to enhanced scintillation

to the location where the enhanced GNSS scintillation occurred. It is reasonable to assume that the EPBs were positioned higher than the LEO satellite's altitude (550 km) or far from the LEO satellite pass, as the beacon signal did not encounter any plasma irregularities. Figure 6 shows the stable relative TEC without significant fluctuations along the pass of LEO satellite.

Case 3: scintillations of beacon signals only (DOY 279, 2021)

On 6 October 2021 (DOY 279), we observed an event where only the beacon signal from the LEO F7/CS FM6 satellite experienced enhanced scintillations, known as Case 3. This occurred between 16:24:18 and 16:27:07 UTC (23:24:18–23:37:07 LT) as shown in Fig. 7a. Interestingly, the beacon signal showed strong S_4 values between longitudes 98.26° to 100.01°, but

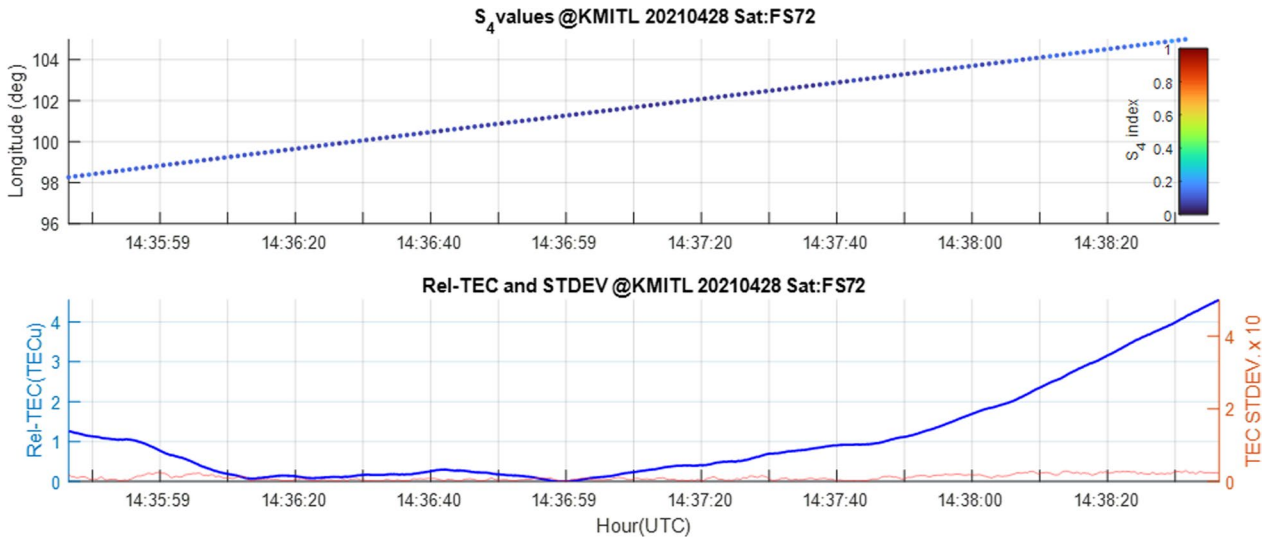

Fig. 6 S_4 index (top) values against the IPP along the LEO satellite's trajectory vs UTC time, the time profile plots of the relative TEC value and its standard deviation (bottom) during the satellite pass between 14:35:49 and 14:38:39 UTC (21:35:49–21:38:39 LT) on 28 April 2021 (DOY 118)

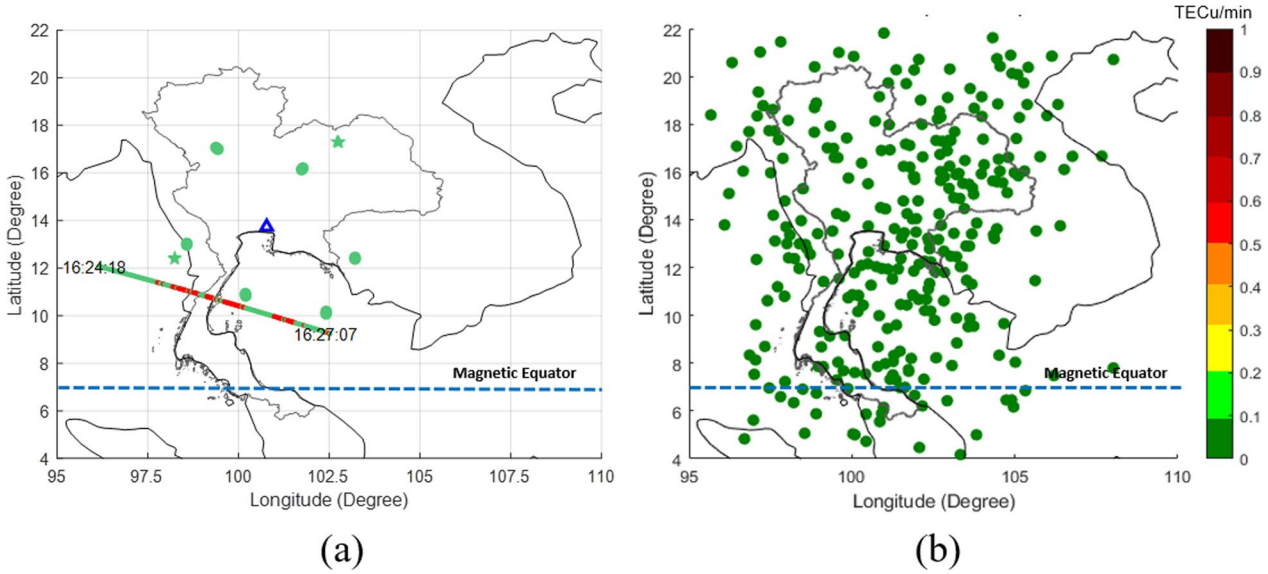

Fig. 7 Maps of ionospheric pierce points (IPPs) of **a** S_4 index of GNSS and LEO satellite signals received at the KMITL Bangkok station and **b** ROTI map of GNSS signals from the KMITL's receiver network over Thailand around 16:25 UTC (23:25 LT) on 06 October 2021 (DOY 279).and red IPPs refer to enhanced scintillations (higher than the threshold)

no scintillations were observed on GNSS signals. This indicates the presence of a large structure of ionospheric instability spanning approximately 300 km of longitudinal width, which occurred near the magnetic equator around midnight. This finding is consistent with the fact that no significant GNSS scintillations caused by EPB are normally detected post-midnight (Otsuka 2018; Li et al. 2021). Figure 7b shows low ROTI values measured by GNSS signals (below 0.1 TECu/min) for all IPPs, indicating the absence of EPBs during this time. Therefore, the results suggest that this LEO's beacon signal scintillation event may have been caused by bottom-side irregularities/structuring of the ionosphere's F region, likely initiated around midnight or post-midnight, without evolving to a higher altitude to fully develop into an EPB. However, further investigations are still required to confirm this assumption. It is hypothesized that irregularities with intermediate-scale sizes of approximately 725 m generated scintillations on the LEO's beacon signals. Figure 8 reveals a strong correlation between the scintillation and the relative

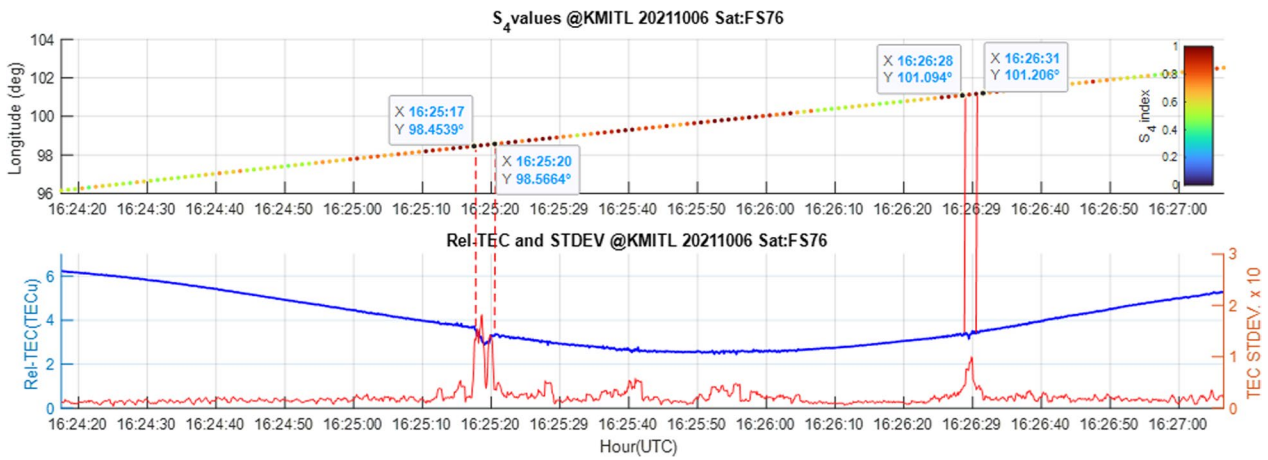

Fig. 8 S_4 index (top) values against the IPP along the LEO satellite's trajectory vs UTC time, the time profile plots of the relative TEC value and its standard deviation (bottom) during the satellite pass between 16:24 and 16:27 UTC (23:24 and 23:27 LT) on 06 October 2021 (DOY 279)

TEC fluctuation from the beacon signal. Scintillation events occurred during periods of notable TEC perturbations. There are two abrupt density-depleted regions with size of 10 km and 2 km.

Summary of all cases

In this work, we examined the scintillation S_4 indices of the LEO F7/C2 satellite's beacon signals at 400 MHz and GNSS L1/E1 signals at 1575.42 MHz recorded at the KMITL Bangkok station in the low-latitude region. The enhanced scintillations on the GNSS L1/E1 signal in Case 1 and Case 2 suggest that the estimated scale sizes of EPB irregularities were approximately 370 m, while Case 3 indicates that the LEO's beacon signal scintillations were caused by bottom-side ionospheric regularities with a scale size approximately 725 m. We interpret that the scintillation effects on the GNSS signal alone in Case 2 occurred when the EPBs were located higher than the LEO satellite's orbit altitude of 550 km or far from the LOE satellite pass. The enhanced scintillation period along the pass of the LEO satellite approximated the longitudinal width of the plasma-depleted region associated with EPBs or bottom-side ionospheric instabilities after midnight, estimated to be 270 km in Case 1, and 300 km in Case 3.

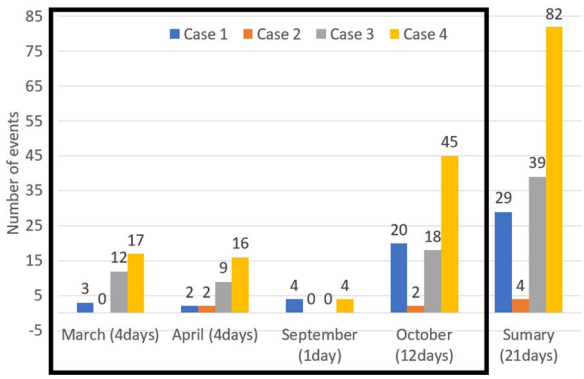

Fig. 9 The frequency of the scintillation events for Cases 1, 2, 3 and 4 for each month and all observation days

We analyzed the statistics of Cases 1 to 4 at the KMITL Bangkok station in 2021. A total of 154 events of the LEO F7/C2 satellites passes were recorded on 21 days in March (4 days), April (4 days), September (1 days), and October (12 days) of 2021 (a low-solar activity year). These events include the 'No scintillation' case (Case 4), which is the largest number events recorded due to the solar minimum year. The bar chart in Fig. 9 shows the frequency distribution of Cases 1, 2, 3, and 4. Scintillations on the LEO satellite's beacon signal with lower frequency were more frequently detected each month compared to scintillations on the GNSS satellite's L1/E1 signals with a higher frequency, as expected. Case 2 exhibited the lowest frequency of scintillation events.

Finally, we examined the occurrence time of the scintillation events of Cases 1, 2, and 3, both of which involve scintillations of the beacon signals as depicted in Fig. 10. The shaded area indicates the post-midnight period. The findings indicate that scintillations on the beacon signal persist until post-midnight (20:00 UTC/next day 3:00 LT) as discussed in (Otsuka 2018; Li et al. 2021). In contrast, scintillations on the GNSS L1/E1 signals triggered by small-scale irregularities of EPBs only occurred before midnight time in the low-latitude region, consistent with previous studies in (Otsuka et al. 2009; Watthanasangmechai et al. 2016). These observations suggest that plasma bubbles with small-scale sizes close to the first Fresnel zone of the GNSS signal decay before midnight, and the large-scale plasma irregularities near pre-dawn do not generate scintillations on the GNSS signal.

Conclusion

This study estimated the scale sizes of equatorial ionospheric irregularities embedded in EPBs using amplitude scintillation S_4 indices of the LEO F7/C2 satellite's beacon signal at a frequency of 400 MHz and the GNSS satellite's L1 or E1 signals with a frequency of 1575.42 MHz recorded by the GRBR and GNSS receivers at the KMITL Bangkok station, Thailand, in the low-latitude region during magnetically quiet condition (Kp < 3). For each LEO satellite pass during the nighttime period, we examined the scintillation S_4 indices of both the beacon and GNSS signals in 2021 and categorized the events into four cases depending on the presence and absence of the scintillations on signals. Enhanced scintillation example events reveal that the longitudinal widths of the EPB's depleted region are estimated to be ~ 260 km in the case of scintillations on both GNSS signal and beacon signal, and ~ 300 km in the case of scintillations on beacon signal only.

The findings are:

- Scintillation effects on GNSS alone are the least frequent.
- Scale sizes of irregularities are approximately 370 m in most post-sunset EPBs.
- Scintillation effects on both GNSS and LEO beacon signals occur only before midnight, while scintillation effects on LEO beacon signals can occur in both pre- and post-midnight.
- Post-sunset scintillation on LEO satellite's beacon signal alone is possibly attributed to the onset of

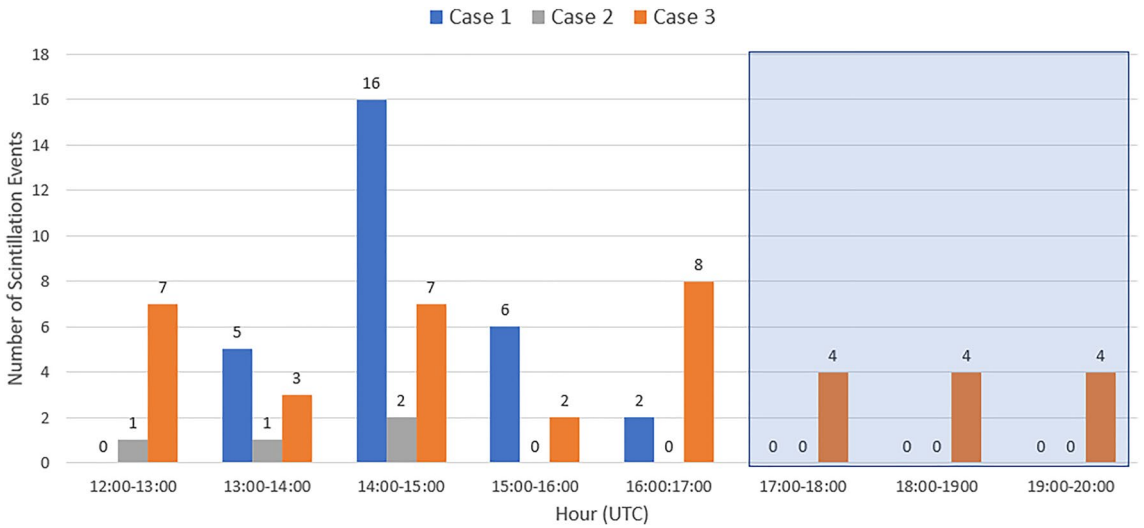

Fig. 10 The occurrence time of the scintillation events related to cases 1, 2 and 3 from 12:00 to 20:00 UTC (19:00–03:00 LT) (the shaded color shows the period after midnight)

developing equatorial plasma bubbles (EPBs) that are not fully developed yet.

- LEO's beacon signal scintillations are observed post-midnight, while no GNSS signal scintillation is detected. These findings suggest a potential link between the observed LEO scintillation and the presence of bottom-side irregularities. However, further investigation with additional data is needed to substantiate this hypothesis.

Moreover, the work also presents the temporal characteristics of the scintillation events that occurred in the low-latitude region in Thailand. In future work, we will study the features of the equatorial ionospheric irregularities including post-sunset EPB and post-midnight bottom-side instability based on the scintillations on LEO and GNSS signals from more stations in Thailand. In addition, similar studies on the days of global disturbances (Kp > 4) during the solar maximum years should be investigated.

Abbreviations

EPB	Equatorial plasma bubble
GNSS	Global Navigation Satellite System
GRBR	GNU Radio Beacon Receiver
KMITL	King Mongkut's Institute of Technology Ladkrabang
NICT	National Institute of Information and Communications Technology
LEO	Low earth orbit
MEO	Medium earth orbit
TEC	Total electron content
ROTI	The rate of the TEC index
VHF	Very high frequency
UHF	Ultra high frequency

Acknowledgements
This work is partially funded by the NSRF via the Program Management Unit for the Human Resources and Institutional Development, Research and Innovation (Grant number B05F640197). The ASEAN IVO (http://www.nict.go.jp/en/asean_ivo/index.html) project, [GNSS and Ionospheric Data Products for Disaster Prevention and Aviation in Magnetic Low-Latitude Regions (Phase II)], was also involved in the production of the contents of this work and financially supported by NICT (http://www.nict.go.jp/en/index.html). We thank Kyoto University, Japan, and the National Institute of Maritime, Port and Aviation Technology, Japan, for supporting the research equipment.

Author's contribution
KS conducted experiments, analyzed and interpreted results. LMMM analyzed and interpreted the results, and wrote the first draft of the paper. KH contributed to the interpretation of scintillation observations. MN provided comments and corrections. SS contributed to the discussion and interpretation of GNSS scintillation observations at KMITL. MR facilitated LEO satellite data sharing and provided methodological implementations. PS supported consultation, methodological implementations, comments, and corrections. All authors have read and approved the final manuscript.

Funding
Not applicable.

Availability of data and materials
The GNSS satellite data used in this manuscript is accessible at the Thai GNSS and Space Weather Information Center, http://iono-gnss.kmitl.ac.th/. The GRBR receiver data is publicly available at https://www.rish.kyoto-u.ac.jp/~yamamoto/digitalbeacon/.

Declarations

Competing interest
There is no competing interests to disclose.

Author details
[1]School of Engineering, King Mongkut's Institute of Technology Ladkrabang, Bangkok 10520, Thailand. [2]National Institute of Information and Communications Technology, Koganei, Tokyo 184-8795, Japan. [3]Electronic Navigation Research Institute, National Institute of Maritime, Port and Aviation Technology, Tokyo 182-0012, Japan. [4]Research Institute for Sustainable Humanosphere, Kyoto University, Uji, Kyoto 611-011, Japan.

Received: 13 May 2023 Accepted: 30 July 2023
Published online: 23 August 2023

References

Abadi P, Saito S, Srigutomo W (2014) Low-latitude scintillation occurrences around the equatorial anomaly crest over Indonesia. Ann Geophys 32:7–17. https://doi.org/10.5194/angeo-32-7-2014

Bhattacharyya A (2022) Equatorial plasma bubbles: a review. Atmosphere 13:1637. https://doi.org/10.3390/atmos13101637

Bhattacharyya A, Beach TL, Basu S, Kintner PM (2000) Nighttime equatorial ionosphere: GPS scintillations and differential carrier phase fluctuations. Radio Sci 35:209–224. https://doi.org/10.1029/1999RS002213

Buhari SM, Abdullah M, Hasbi AM et al (2014) Continuous generation and two-dimensional structure of equatorial plasma bubbles observed by high-density GPS receivers in Southeast Asia. J Geophys Res Space Phys 119:569–580. https://doi.org/10.1002/2014JA020433

Bumrungkit A, Supnithi P, Saito S, Myint LMM (2022) A study of equatorial plasma bubble structure using VHF radar and GNSS scintillations over the low-latitude regions. GPS Solut 26:148. https://doi.org/10.1007/s10291-022-01321-4

de Oliveira MA, da Silveira RF, Perrella WJ, de Paula ER (2012) Analysis of the characteristics of low-latitude GPS amplitude scintillation measured during solar maximum conditions and implications for receiver performance. Surv Geophys 33:1107–1131. https://doi.org/10.1007/s10712-011-9161-z

Ghobadi H, Spogli L, Alfonsi L et al (2020) Disentangling ionospheric refraction and diffraction effects in GNSS raw phase through fast iterative filtering technique. GPS Solut 24:85. https://doi.org/10.1007/s10291-020-01001-1

Groves KM, Basu S, Weber EJ et al (1997) Equatorial scintillation and systems support. Radio Sci 32:2047–2064. https://doi.org/10.1029/97RS00836

Hsiao TY, Huang C, Yeh W-H et al (2022) The observations of localize ionospheric scintillation structure by FORMOSAT-7/COSMIC-2 Tri-band Beacon network. Terr Atmos Ocea Sci 33:10. https://doi.org/10.1007/s44195-022-00010-6

Joshi LM, Tsai L-C, Su S-Y et al (2019) Investigation of spatiotemporal morphology of plasma bubbles based on EAR observations. J Geophys Res Space Phys 124:10549–10563. https://doi.org/10.1029/2019JA026839

Kintner PM, Humphreys T, Hinks J (2009) GNSS and ionospheric scintillation—How to survive to the next solar maximum. Inside GNSS. 4:22–30. https://www.insidegnss.com/auto/julyaug09-kintner.pdf. Accessed 8 Mar 2023

Krypiak-Gregorczyk A, Wielgosz P (2018) Carrier phase bias estimation of geometry-free linear combination of GNSS signals for ionospheric TEC modeling. GPS Solut 22:45. https://doi.org/10.1007/s10291-018-0711-4

Li G, Ning B, Otsuka Y et al (2021) Challenges to equatorial plasma bubble and ionospheric scintillation short-term forecasting and future aspects in East and Southeast Asia. Surv Geophys 42:201–238. https://doi.org/10.1007/s10712-020-09613-5

Liow YY, Buhari SM, Abdullah M, et al (2019) The observation of ionospheric large-scale wave structure in Southeast Asia. In: 2019 6th International Conference on Space Science and Communication (IconSpace). IEEE, p 192–196. https://doi.org/10.1109/IconSpace.2019.8905972

Manga NA, Lakshmanna K, Sarma AD, Pant TK (2021) Analysis of correlation between ROTI and S4 using Gagan data. Progress Electromagn Res M 99:23–34. https://doi.org/10.2528/PIERM20101405

Oliveira Moraes A, Costa E, Abdu MA et al (2017) The variability of low-latitude ionospheric amplitude and phase scintillation detected by a triple-frequency GPS receiver. Radio Sci 52:439–460. https://doi.org/10.1002/2016RS006165

Otsuka Y (2018) Review of the generation mechanisms of post-midnight irregularities in the equatorial and low-latitude ionosphere. Prog Earth Planet Sci 5:57. https://doi.org/10.1186/s40645-018-0212-7

Otsuka Y, Ogawa T, Effendy (2009) VHF radar observations of nighttime F-region field-aligned irregularities over Kototabang, Indonesia. Earth Planet Space 61:431–437. https://doi.org/10.1186/BF03353159

Pi X, Mannucci AJ, Lindqwister UJ, Ho CM (1997) Monitoring of global ionospheric irregularities using the Worldwide GPS Network. Geophys Res Lett 24:2283–2286. https://doi.org/10.1029/97GL02273

Rama Rao PVS, Gopi Krishna S, Niranjan K, Prasad DSVVD (2006) Study of spatial and temporal characteristics of L-band scintillations over the Indian low-latitude region and their possible effects on GPS navigation. Ann Geophys 24:1567–1580. https://doi.org/10.5194/angeo-24-1567-2006

Salles LA, Vani BC, Moraes A et al (2021) Investigating ionospheric scintillation effects on multifrequency GPS signals. Surv Geophys 42:999–1025. https://doi.org/10.1007/s10712-021-09643-7

Seechai K, Myint LMM, Hozumi K, Supnithi P (2022) Comparison study of amplitude scintillation between GNSS and satellite beacon receivers in Thailand. In: 2022 37th International Technical Conference on Circuits/Systems, Computers and Communications (ITC-CSCC). IEEE, p 1–4. https://doi.org/10.1109/ITC-CSCC55581.2022.9894879

Taiwan Space Agency (2023) FORMOSAT-7/COSMIC-2. https://www.tasa.org.tw/inprogress.php?c=20022301&ln=en. Accessed 8 Mar 2023

Tsunoda RT (2015) Upwelling: a unit of disturbance in equatorial spread F. Prog Earth Planet Sci 2:9. https://doi.org/10.1186/s40645-015-0038-5

Watthanasangmechai K, Yamamoto M, Saito A et al (2014) Latitudinal GRBR-TEC estimation in Southeast Asia region based on the two-station method. Radio Sci 49:910–920. https://doi.org/10.1002/2013RS005347

Watthanasangmechai K, Yamamoto M, Saito A et al (2016) Predawn plasma bubble cluster observed in Southeast Asia. J Geophys Res Space Phys 121:5868–5879. https://doi.org/10.1002/2015JA022069

Xiong B, Wan W-X, Ning B-Q et al (2007) A comparison and analysis of the S_4 index, C/N and Roti over Sanya. Chin J Geophys 50:1414–1424. https://doi.org/10.1002/cjg2.1161

Yamamoto M (2008) Digital beacon receiver for ionospheric TEC measurement developed with GNU Radio. Earth Planet Space 60:e21–e24. https://doi.org/10.1186/BF03353137

Yang Z, Liu Z (2016) Correlation between ROTI and ionospheric scintillation indices using Hong Kong low-latitude GPS data. GPS Solut 20:815–824. https://doi.org/10.1007/s10291-015-0492-y

Yeh KC, Liu C-H (1982) Radio wave scintillations in the ionosphere. Proc IEEE 70:324–360. https://doi.org/10.1109/PROC.1982.12313

Yokoyama T, Shinagawa H, Jin H (2014) Nonlinear growth, bifurcation, and pinching of equatorial plasma bubble simulated by three-dimensional high-resolution bubble model. J Geophys Res Space Phys 119:10474–10482. https://doi.org/10.1002/2014JA020708

Publisher's Note